THE JOURNAL OF PHYSICAL CHEMISTRY B

Article

pubs.acs.org/JPCB

Oxidation Dynamics of Methionine with Singlet Oxygen: Effects of Methionine Ionization and Microsolvation

Fangwei Liu and Jianbo Liu*

Department of Chemistry and Biochemistry, Queens College and the Graduate Center of the City University of New York, Queens, New York 11367, United States

Supporting Information

ABSTRACT: We report an in-depth study on the gas-phase reactions of singlet $O_2[a^1\Delta_g]$ with methionine (Met) at different ionization and hydration states (including deprotonated $[Met - H]^-$, hydrated deprotonated $[Met - H]^-(H_2O)_{1,2}$, and hydrated protonated $MetH^+(H_2O)_{1,2}$), using guided-ion-beam scattering mass spectrometry. The measurements include the effects of collision energy (E_{col}) on reaction cross sections over a center-of-mass E_{col} range from 0.05 to 1.0 eV. The aim of this study is to probe the influences of Met ionization and hydration on its oxidation mechanism and dynamics. Density functional theory calculations, Rice-Ramsperger-Kassel-Marcus modeling, and quasi-classical, direct dynamics trajectory simulations were performed to examine the properties of various complexes and transition states that might be important along reaction coordinates, probe reaction potential energy surfaces, and to establish the atomic-level mechanism for the Met oxidation process. No oxidation products were observed for the reaction of $[Met - H]^-$ with $^1O_2$ due to the high-energy barriers located in the product channels for this system. However, this nonreactive property was altered by the microsolvation of $[Met - H]^-$; as a result, hydroperoxides were captured as the oxidation products for $[Met - H]^-(H_2O)_{1,2} + {}^1O_2$. For the reaction of $MetH^+(H_2O)_{1,2} + {}^1O_2$, besides formation of hydroperoxides, an H_2O_2 elimination channel was observed. The latter channel is similar to what was found in the reaction of dehydrated $MetH^+$ with $^1O_2$ (*J. Phys. Chem. B* **2011**, *115*, 2671). The reactions of hydrated protonated and deprotonated Met are all inhibited by E_{col}, becoming negligible at $E_{col} \geq 0.5$ eV. The kinetic and dynamical consequences of microsolvation on Met oxidation and their biological implications are discussed.

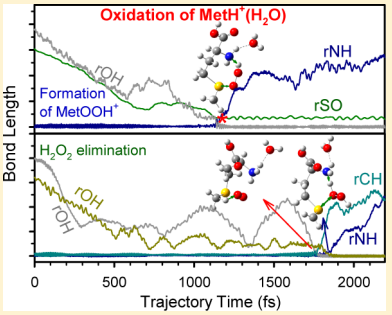

1. INTRODUCTION

Singlet O_2 $[a^1\Delta_g]$ is a reactive oxygen species,[1] which can be produced in biological systems via energy transfer to ground-state triplet O_2 $[X^3\Sigma_g]$ from protein-bound or other chromophores on exposure to UV and/or visible light (i.e., photosensitization[2]) or by a range of enzymatic and non-enzymatic reactions.[3] Proteins are a major target for $^1O_2$-mediated oxidative damage in living bodies, with damage occurring preferentially at tryptophan (Trp), histidine (His), tyrosine (Tyr), methionine (Met), and cysteine (Cys) residues because these residues have electron-rich side chains.[3−5]

Met is structurally important in many enzymes (e.g., yeast enolase, lysozyme, ribonuclease A, and phosphoglucomutase).[6] Hydrophobic contacts via the Met residue contribute to protein stability. Moreover, Met has the propensity to interact with aromatic-containing residues, and the resulting Met sulfur-aromatic motif provides additional stabilization over hydrophobic interactions.[7] Oxidation of Met to Met sulfoxide MetO[8,9] decreases hydrophobicity and disrupts both dispersion and electrostatic interactions present in the sulfur-aromatic motif. This oxidation-induced post-translational modification affects the conformations of proteins.[7,10] The ensuring tertiary structural rearrangements may cause proteins to lose functions[11−13] and are related to several pathophysiological conditions such as cancer, aging, and neurodegenerative diseases.[5,10,14]

One characteristic feature of Met oxidation is that cells develop a counteract process to reduce the MetO residues. This repair process is catalyzed by methionine sulfoxide reductases (Msrs).[15−17] The thioredoxin-dependent reduction of MetO is an evolutionary response to oxygen-induced damage in the Earth's atmosphere and in more localized environments.[14,18] Consequently, oxidation of Met can be made use of as an antioxidant pool. Particularly, surface-exposed Met residues may protect other residues under oxidative stress,[19,20] and the increase of oxidized Met residues in proteins indicates an increase of $^1O_2$ (and other reactive oxygen species) generation, decrease of oxidant scavengers, or loss of Msrs' activities and other reducing equivalents involved. For these reasons, Met oxidation has been investigated extensively by biologists and biochemists. Many experiments[6,21−27] are focused on or related to photodynamic actions[28] and were carried out in solution using photooxidation methods[2] where $^1O_2$ was generated by sensitizers.

Received: April 20, 2015
Revised: May 21, 2015
Published: May 22, 2015

DOI: 10.1021/acs.jpcb.5b03779
J. Phys. Chem. B 2015, 119, 8001−8012

In a previous study, we reported the reaction of "bare" protonated $MetH^+$ with $^1O_2$ in the gas phase.[29] The reaction produces hydrogen peroxide and a dehydro compound of $MetH^+$ via transfer of two H atoms from $MetH^+$ to $^1O_2$. Our experiment was carried out in a guided-ion-beam apparatus, where the reaction system was separated from bulk solution environments. All the complexities associated with solution-phase photooxidations (e.g., pH, O_2 concentration, solvent composition, combination of light and sensitizers, and competition between radical- and $^1O_2$-mediated reactions) were avoided in the gas phase. Accordingly, the intrinsic reactivity of Met was distinguished from solvent and counterion effects.

Another effort in our gas-phase experiments is to make these reactions closely correlated to and resemble the oxidation reactions in solution, so that we may extrapolate gas-phase findings to biological systems. Amino acids are able to form hydrogen bonds with water molecules,[30] and the presence of hydrogen-bonded water is critical for molecular dynamics.[31] Theoretically, the intrinsic properties of amino acids and the effects caused by the interaction with water can be distinguished by a comparison of gas- and solution-phase reaction products. But a simple comparison of gas- and solution-phase reactions may not be able to reveal the effects of individual water molecules on amino acid oxidation. Our approach is to hydrate amino acid ions in the gas phase using electrospray ionization (ESI)[32] and study the reactions of resulting gas-phase hydrates as a function of hydration number.

The comparison between the $^1O_2$ oxidation of bare protonated/deprotonated His and their hydrated species in our recent work exemplifies the importance of individual water ligand(s) in manipulating amino acid reactivity.[33] The reaction of dehydrated protonated $HisH^+$ with $^1O_2$ leads to no products. The origin of this nonreactivity was revealed on the basis of reaction potential energy surface (PES) calculations, statistical modeling, and dynamics simulations. It was found that the reaction intermediates (i.e., endoperoxide His-2,5-OO^+ and hydroperoxide His-5-OOH^+) carried high internal energy and therefore are destined to decomposition; however, all product channels were blocked by high activation barriers, so both intermediates ultimately decayed back to reactants. A similar nonreactive scenario occurred to the reaction of deprotonated $[His - H]^-$ with $^1O_2$. Interestingly, stable hydroperoxide products were captured once $HisH^+$ and $[His - H]^-$ became microsolvated with water. This suggests that "hot" endoperoxide and hydroperoxide intermediates can remove internal excitation by evaporating water ligand(s) and becoming stabilized. Moreover, the reaction efficiency of $[His - H]^-$ hydrates was found to be much higher than that of the protonated ones. This observation mimics the pH dependence observed in the solution-phase photooxidation of His.[22,34]

The $^1O_2$ oxidation of Cys suffices as another illustration of the consequence of microsolvation on oxidation dynamics.[35−37] The oxidation of bare Cys (either protonated or deprotonated) dumped reaction exoergicity into products and caused fragmentation of the Cys moiety. Nevertheless, the addition of water ligand(s) to the system suppressed product decomposition and intrinsically influenced oxidation pathways. Pathways that are otherwise not likely in the gas phase become feasible in Cys-water clusters. These findings reinforce the understanding that gas-phase hydrated amino acids involve individual solute−solvent dynamics and their coupling, rather than simply amino acid dynamics under the influence of some representation of the solvent.

In the present paper, we first investigate the reaction of bare deprotonated $[Met - H]^-$ with $^1O_2$. Comparison of $[Met - H]^- + {}^1O_2$ with $MetH^+ + {}^1O_2$[29] demonstrates ionization effects on Met oxidation dynamics. We then explore the $^1O_2$ oxidation of hydrated Met in both protonated and deprotonated states. Reaction products and cross sections of $MetH^+(H_2O)_n$ and $[Met - H]^-(H_2O)_n$ were measured as a function of hydration number. As a result, the effects of individual solvent molecules were revealed, and the transition of Met oxidation chemistry from the gas phase to aqueous solution can be sensed.

2. EXPERIMENTAL AND COMPUTATIONAL DETAILS

2.1. Ion−Molecule Scattering of $[MetH^+](H_2O)_{1-2}$ and $[Met - H]^-(H_2O)_{0-2}$ with $^1O_2$. Gas-phase reactions were performed using a homemade guided-ion-beam tandem mass spectrometer, which was described in detail previously,[38] along with the operation, calibration, and data analysis procedures. The apparatus consists of an ion-source, radio frequency (rf) hexapole ion guide, quadrupole mass filter, rf octopole ion guide surrounded by a scattering cell, second quadrupole mass filter, and a pulse-counting detector. Both quadrupole mass filters were operated at 2.1 MHz to cover a mass/charge (m/z) range of 1−500.

A sample solution for generating $MetH^+$ was prepared in HPLC-grade methanol/water (1:1 vol ratio) containing 0.5 mM L-methionine (≥99.5%, Sigma-Aldrich) and equimolar HCl, and that for $[Met - H]^-$ was prepared in methanol/water (4:1) containing 0.5 mM L-methionine and 0.5 mM NaOH. The solution was sprayed into the ambient atmosphere through an electrospray needle at a flow rate of 0.03−0.05 mL/h. The ESI needle was held at 2.3 and −2.0 kV for producing positively and negatively charged species, respectively. Charged droplets entered the source chamber of the mass spectrometer through a desolvation capillary. The capillary was held at 100 to 120 V for positive ions and −120 to −150 V for negative ions. Liquid droplets underwent desolvation as they passed through the heated capillary, converting to gas-phase ions in the source chamber. Under mild heating conditions, not all of the solvent was evaporated, resulting in hydrated ions. In the experiment, the capillary was heated to 180 °C for generating dehydrated ions, 132−134 °C for monohydrated ions and 120−130 °C for dihydrated ions.

A skimmer with an orifice of 0.99 mm is located 3 mm from the capillary end, separating the source chamber and the hexapole ion guide. The skimmer was biased at 20 V for positive ions and −20 V for negative ions. Ions were transported into the hexapole at a pressure of 24 mTorr and underwent collisional focusing and cooling to ∼310 K. Ions subsequently passed into a conventional quadrupole for selection of specific reactant ions. Reactant ions were collected and focused into the octopole ion guide, which trapped ions in the radical direction, minimizing loss of the reactant and product ions resulting from scattering. The octopole is surrounded by the scattering cell containing neutral reactant gas. The cell pressure was measured by a Baratron capacitance manometer (MKS 690 head and 670 signal conditioner).

After passing through the scattering cell, remaining reactant ions and product ions drifted to the end of the octopole, mass analyzed by the second quadrupole, and counted. The kinetic energy of the reactant ions in the laboratory frame (E_{lab}) was controlled by a DC bias voltage applied to the octopole. E_{lab}

DOI: 10.1021/acs.jpcb.5b03779
J. Phys. Chem. B 2015, 119, 8001−8012

can be converted into the collision energy (E_{col}) between ions and $^1O_2$ molecules in the center-of-mass frame using $E_{col} = E_{lab} \times m_{neutral}/(m_{ion} + m_{neutral})$, where $m_{neutral}$ and m_{ion} are the masses of neutral and ionic reactants, respectively. Reaction cross sections at different E_{col} were calculated from the ratios of reactant and product ion intensities (under single ion−molecule collision conditions), the pressure of $^1O_2$ in the scattering cell (= the total gas pressure in the cell × the fractional abundance of $^1O_2$), and the effective cell length. The scattering cell pressure was set at 0.28 mTorr containing 5% of $^1O_2/^3O_2$ and 95% of He. Under these conditions, Met ions underwent at most a single collision with O_2. Met ions also collided with He, but heavy ion-light neutral combination made these collisions insignificant at low E_{col}.

$^1O_2$ was generated by the reaction of $H_2O_2 + Cl_2 + 2KOH \rightarrow {}^1O_2/{}^3O_2 + 2KCl + 2H_2O$.[29,39] In the experiment, 13 mL of 8 M KOH was added to 20 mL of 35 wt % aqueous H_2O_2 in a sparger held at −19 °C, and the resulting mixture was degassed. 2.6 sccm of Cl_2 (~99.5%, Sigma-Aldrich) was mixed with 50 sccm of He and bubbled through the H_2O_2/KOH slush. All of the Cl_2 reacted with H_2O_2 to produce the product mixture of ground and excited electronic state O_2 and water.[39] The gas products passed through a cold trap (kept at −70 °C) to remove water vapor. Only $^1O_2$, $^3O_2$, and He remained in the downstream gas. Before leaking into the scattering cell, the concentration of $^1O_2$ in the gas was determined by measuring $^1O_2$ emission ($a^1\Delta_g \rightarrow X^3\Sigma_g$, $v = 0-0$)[40] at 1270 nm in an optical emission cell. Emission from the cell passed through an optical chopper (SRS model SR540) and a 5 nm bandwidth interference filter centered at 1270 nm and was focused into a thermoelectrically cooled InGaAs detector (Newport 71887) coupled with a lock-in amplifier (SRS model SR830). The amplifier output was converted to absolute $^1O_2$ concentration based on a previous calibration.[41] To maintain a steady-state $^1O_2$ concentration, the $^1O_2$ generator was continuously pumped with a mechanical pump to 25 τ through a pressure relay. The intensity of $^1O_2$ emission was monitored continuously during the experiment, and signal variation (controlled to be within 20%) was corrected for ion−molecule cross sections. The entire experiment was repeated multiple times, and each time we cycled through different E_{col}. The data presented are averages of several complete data sets. To check the reactivity of $MetH^+(H_2O)_{1-2}$ and $[Met - H]^-(H_2O)_{0-2}$ toward $^3O_2$/He, control experiments were performed under the same conditions except that Cl_2 was replaced by oxygen gas at the same flow rate.

2.2. Electronic Structure Calculations, Statistical Modeling, and Dynamics Simulations. Geometries of reactants, intermediates, transition states (TSs) and products were optimized using Gaussian 09,[42] at the B3LYP level of theory with 6-31+G(d) and 6-311++G(d,p) basis sets. Conformation searching was conducted for all reactant ions and their hydrates, and their most stable conformations were used as the starting structures in reaction coordinates, statistical modeling, and trajectories. All TSs were verified as first-order saddle points, and the vibrational mode with an imaginary frequency corresponds to the associated reaction pathway. Density functional theory (DFT)-calculated vibrational frequencies and zero-point energies (ZPEs) were scaled by a factor of 0.952 and 0.977,[43] respectively. All energies were reported with thermal corrections at 298 K (including ZPE). Rice-Ramsperger-Kassel-Marcus (RRKM)[44] rates were calculated with the program of Zhu and Hase,[45] using direct state count algorithm and scaled DFT frequencies and energetics.

Direct dynamics simulations for the collisions of $MetH^+(H_2O)$ with $^1O_2$ were carried out at E_{col} = 0.1 and 0.2 eV, using Venus[46] interfaced with Gaussian 09. Considering accuracy and computational cost, the B3LYP/4−31G(d) level of theory was chosen for trajectory integration. The initial separation between $MetH^+(H_2O)$ and $^1O_2$ was set at 8.0 Å (where the attractive potential between the reactants is only a few meV), with a collision impact parameter of 0.1 Å. The vibrational and rotational temperatures of all reactants were set at 300 K, which were chosen to mimic our experiment. Quasi-classical Boltzmann sampling[47] was used to select vibrational and rotational energies.

The Hessian-based predictor-corrector algorithm[48] was used for numerical integration of the classical equations of motion, with the Hessian matrix updated every five steps. A step size of 0.25 $amu^{1/2}$Bohr (corresponding to a step size of 0.5 - 0.6 fs in trajectory time) was used for trajectories. The initial guess of molecular orbital for each DFT calculation was obtained from the previous step, and the total energy of the system was checked during the simulation to ensure that the energy was conserved to better than 10^{-4} Hartree. The SCF = XQC option was adopted for the trajectory integration so that a quadratically convergent SCF method was used in case the conventional first-order SCF algorithm failed to converge within allotted cycles. Trajectories were terminated when the product separation exceeded 8.1 Å. gOpenMol[49] was used for trajectory visualization. Analysis of individual trajectories and statistical analysis of the trajectory ensemble were done using programs written for these purposes.

3. RESULTS AND DISCUSSION

3.1. Structures of $[Met - H]^-$, $[Met - H]^-(H_2O)_{1,2}$, and $MetH^+(H_2O)_{1,2}$. To locate the global minimum in the conformation landscape of $[Met - H]^-$, a similar grid search method used for $MetH^+$[29] conformation optimization was applied. Each of the torsion angles of the Met backbone was rotated systematically through 360° at 60° increments to generate trial staggered conformations for $[Met - H]^-$. Every conformation so generated was subjected to geometry optimization at B3LYP/6-31+G(d) to derive associated local minimum energy conformation. Many of the initial conformations converged to the same local minimum. These conformations were reoptimized using a larger basis set B3LYP/6-311++G(d,p). A total of 9 stable conformers were found for $[Met - H]^-$. The most significant four are depicted in the top row of Figure 1. Each conformer has a number suffix to denote the order of stability, with a percentile population of 54%, 26%, 18%, and 2%, respectively, at 298 K. Our conformation search reproduced the stable deprotonated conformers reported by others.[50]

Starting geometries of monohydrated ions were obtained by adding a water to all possible hydration sites in the lowest energy conformations of $MetH^+$[29] and $[Met - H]^-$ and then optimized at B3LYP/6-311++G(d,p). A similar approach was used to build the hydration shell of other amino acids.[33,37,51,52] Four low-lying conformers were identified for $[Met - H]^-(H_2O)$ and are included in Figure 1. Hydration energy was calculated using $E_{hydration} = E$ (bare ion) + nE (H_2O) − E (cluster), where E (bare ion), E (H_2O), and E (cluster) are the DFT energies of bare ion, water, and the hydrate of the same ion conformation, respectively. Although both the carboxylate

DOI: 10.1021/acs.jpcb.5b03779
J. Phys. Chem. B 2015, 119, 8001−8012

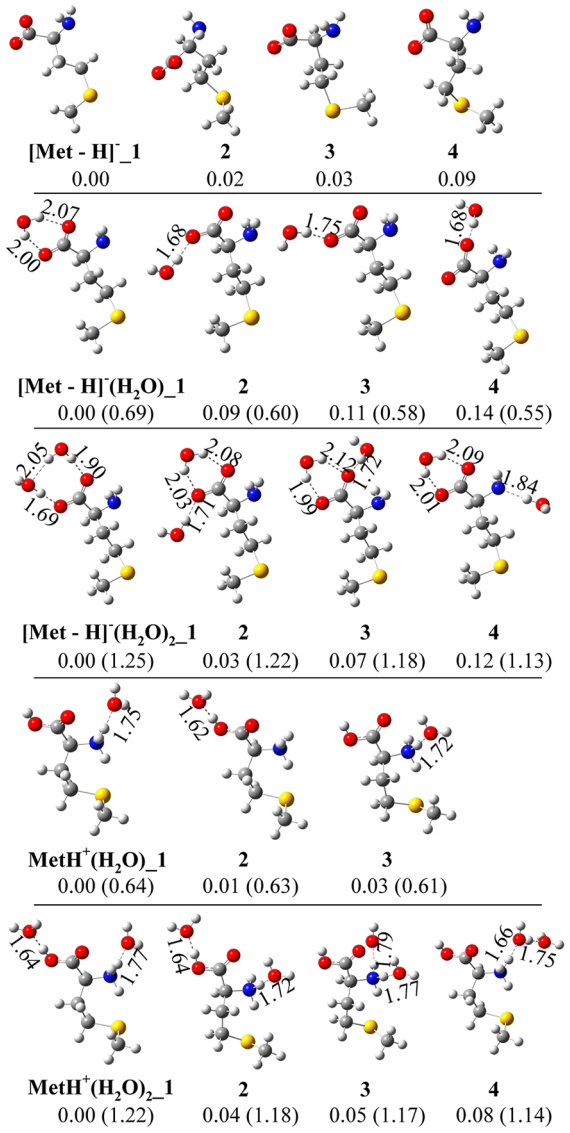

Figure 1. Low-lying conformers of $[Met - H]^-$, $[Met - H]^-(H_2O)_{1,2}$, and $MetH^+(H_2O)_{1,2}$. Dashed lines indicate hydrogen bonds. Bond distances are shown in angstroms. Relative energies (eV, including ZPE) and hydration energies (presented in parentheses) were calculated at B3LYP/6-311++G(d,p).

and amino groups of $[Met - H]^-$ can offer binding sites for water, stable hydrates prefer to have water hydrogen bonded to the carboxylate. The lowest energy conformer, $[Met - H]^-(H_2O)$_1, undergoes bidentate complexation, forming two hydrogen bonds between H_2O and COO^- via a six-membered cyclic arrangement with a hydration energy of 0.69 eV. This conformer accounts for 95% of the monohydrate at 298 K. The other three conformers are monodentate complexes, all forming a single hydrogen bond between H_2O and COO^-, with a total population of 5%.

Starting geometries of $[Met - H]^-(H_2O)_2$ were created by combining any two of the hydration sites we have identified in $[Met - H]^-(H_2O)$. The first four low-lying conformations are shown in Figure 1. The most stable conformer $[Met - H]^-(H_2O)_2$_1 accounts for a 75% population of the dihydrate at 298 K. It has each water form a hydrogen bond with a carboxylate oxygen atom, plus a weaker hydrogen bond between the two waters, with a total $E_{hydration}$ of 1.25 eV. In $[Met - H]^-(H_2O)_2$_2, 3, and 4, one water simultaneously binds to the two O atoms of $-COO^-$ in a manner similar to that in $[Met - H]^-(H_2O)_2$_1, and the other water either binds to an O atom of $-COO^-$ or to the N atom of $-NH_2$.

Three stable conformations were found for $MetH^+(H_2O)$ as shown in Figure 1, with a population of 52%, 33%, and 15%, respectively. Both the carboxyl and ammonium groups of $MetH^+$ offer hydration sites. The water oxygen either binds to the $-OH$ site of the carboxyl group with $E_{hydration}$ of 0.63 eV or binds to one of the three $-NH$ sites of the ammonium group with $E_{hydration}$ of 0.61−0.64 eV. We tried the conformations of HN···HOH···S, where the water bridges the ammonium group and the S atom, but all such starting conformations converged to the most stable conformation $MetH^+(H_2O)$_1.

Structures of $MetH^+(H_2O)_2$ were obtained by adding a second water to each of the stable $MetH^+(H_2O)$ structures. The most stable dihydrate, $MetH^+(H_2O)_2$_1 with a population of 70% at 298 K, has two waters hydrogen-bonded to $-OH$ and $-NH$, respectively. Due to the decreasing effective charge on NH_3^+ and the increasing repulsion between water ligands, the hydration energy of $MetH^+(H_2O)_2$_1 (1.22 eV) is 0.05 eV less than the sum of two corresponding monohydrates [i.e., $MetH^+(H_2O)$_1 (0.64 eV) and $MetH^+(H_2O)$_2 (0.63 eV)]. Our calculated $E_{hydration}$ values agree with Wincel's experiment,[53] which reported $E_{hydration}$ of 0.68 eV for monohydrated $MetH^+$ and 1.32 eV for dihydrated $MetH^+$.

3.2. Reaction Products and Cross Sections. *A. $[Met - H]^- + {}^1O_2$.* Contrary to the high reactivity of $MetH^+$ toward $^1O_2$,[29] no oxidation products were observed for the reaction of dehydrated $[Met - H]^-$ (m/z 148) with $^1O_2$. Only collision-induced dissociation (CID) product ions were observed at high E_{col}, due to elimination of H_2O, CO_2, CH_3SH, and $CH_2CH_2SCH_3$ from $[Met - H]^-$.[54,55]

Note that the electron detachment energy for $[Met - H]^-$ was calculated to be 2.65 eV at the B3LYP/6-31+G(d) level of theory (and electron detachment is accompanied by decarboxylation), which is beyond the E_{col} range of 0.05−1.0 eV used in our experiment. Accordingly, the detachment of the excess electron from $[Met - H]^-$ could not occur during ion−molecule scattering. On the basis of the excitation energy (0.98 eV)[40] and the electron affinity (0.45 eV)[56] of $^1O_2$, electron transfer between $[Met - H]^-$ and $^1O_2$ is endothermic by 1.22 eV and thus cannot occur in our E_{col} range either.

B. $[Met - H]^-(H_2O)_{1,2} + {}^1O_2$. For the reaction of $[Met - H]^-(H_2O)$ (m/z 166) + $^1O_2$, product ions include m/z 47, 75, 130, 133, 148, and 180. Product ions of m/z 47, 75, 130, 133, and 148 correspond to elimination of $H_2NCH(CH_2CH_2)CO_2$, H_2NCHCO_2, CH_3, and H_2O from $[Met - H]^-(H_2O)$ or its daughter ion $[Met - H]^-$, respectively, and their intensities increase at high E_{col}. Among these CID channels, water elimination is the most significant. These product ions were also observed in the collisions of $[Met - H]^-(H_2O)$ with $^3O_2$/He and, therefore, could be excluded from $^1O_2$ chemistry. Product ions of m/z 180, on the other hand, were only observed in the reaction with $^1O_2$ and can be attributed to formation of hydroperoxide $[Me\ t - 2H]OOH^-$. The cross section of m/z 180 is shown in Figure 2a, as a function of the center-of-mass E_{col}. Also shown in the figure is the reaction efficiency (right-hand scale), estimated by $\sigma_{reaction}/\sigma_{collision}$, where $\sigma_{collision}$ is the greater of ion-induced dipole capture cross section[57] and hard-sphere collision cross section.

For the reaction of $[Met - H]^-(H_2O)_2$ (m/z 184) + $^1O_2$, product ions were observed at m/z 47, 75, 130, 133, 148, 180,

DOI: 10.1021/acs.jpcb.5b03779
J. Phys. Chem. B 2015, 119, 8001−8012

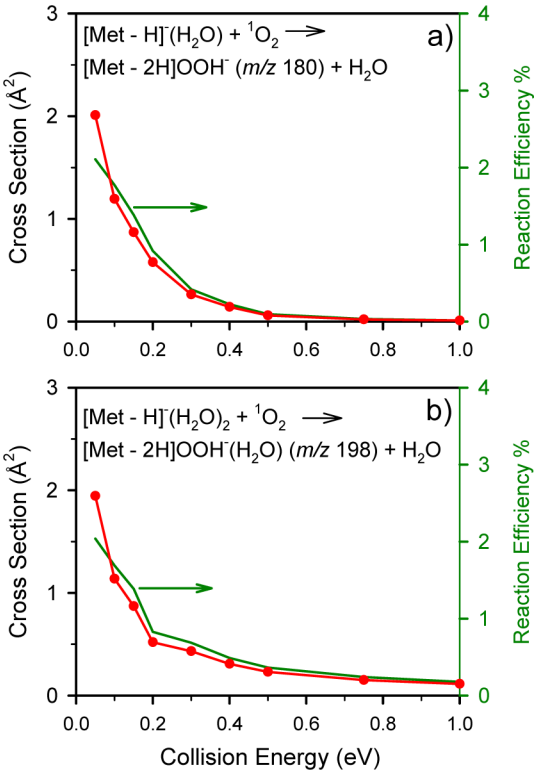

Figure 2. Product cross sections for the reactions of $^1O_2$ with (a) $[Met - H]^-(H_2O)$ and (b) $[Met - H]^-(H_2O)_2$, as a function of E_{col}. Reaction efficiencies (dark green curves) are shown on the right axis using log scale.

and 198. Similar to the reaction of $[Met - H]^-(H_2O) + {}^1O_2$, the product ions of m/z 47, 75, 130, 133, and 148 were produced from CID of $[Met - H]^-(H_2O)_2$. Only the products ions of m/z 180 (only significant at $E_{col} \leq 0.2$ eV) and 198 are attributed to $^1O_2$-specific products $[Met - 2H]OOH^-$ and $[Met - 2H]OOH^-(H_2O)$, respectively. On the basis of the reaction enthalpy calculation (vide infra), formation of dehydrated $[Met - 2H]OOH^-$ appears to be endothermic for $[Met - H]^-(H_2O)_2 + {}^1O_2$ and, therefore, should not be expected in the low-energy regime. However, the $[Met - 2H]OOH^-(H_2O)$ products have low velocities in the lab frame at low E_{col} and are likely to undergo secondary reaction with the neutral gas in the scattering cell, eliminating the remaining water ligand. Consequently, some of $[Met - 2H]OOH^-(H_2O)$ was converted to $[Met - 2H]OOH^-$. To correct for the secondary reactions at low E_{col}, we lumped the intensities of m/z 180 and 198 together in calculating the cross section as well as the reaction efficiency in Figure 2b.

The reactions of $[Met - H]^-(H_2O)_{1,2}$ with $^1O_2$ are inefficient and strongly inhibited by collision energies. Their reaction efficiencies are only ~2% at the lowest E_{col}, becoming negligible at $E_{col} \geq 0.5$ eV. The E_{col} dependence of these reactions suggests that the reactions may be complex-mediated, with complex formation probabilities and/or lifetimes strongly suppressed by E_{col}.

C. $MetH^+(H_2O)_{1,2} + {}^1O_2$. Oxidation products for the reaction of $MetH^+(H_2O)$ (m/z 168) + $^1O_2$ were observed at m/z 148 and 182. The product channel of m/z 148 can be attributed to the abstraction of two H atoms from $MetH^+(H_2O)$ by $^1O_2$ to form hydrogen peroxide, followed by liberation of the water ligand, and is referred to as the H_2O_2 channel. A similar H_2O_2 channel was observed for the reaction of $MetH^+ + {}^1O_2$.[29] The product channel of m/z 182 corresponds to formation of $MetOOH^+$ by elimination of the H_2O ligand from the reaction intermediate $MetOOH^+(H_2O)$. Cross sections for the two product channels and the total reaction efficiencies are shown in Figure 3a over the E_{col} range from 0.1 to 1.0 eV. The cross

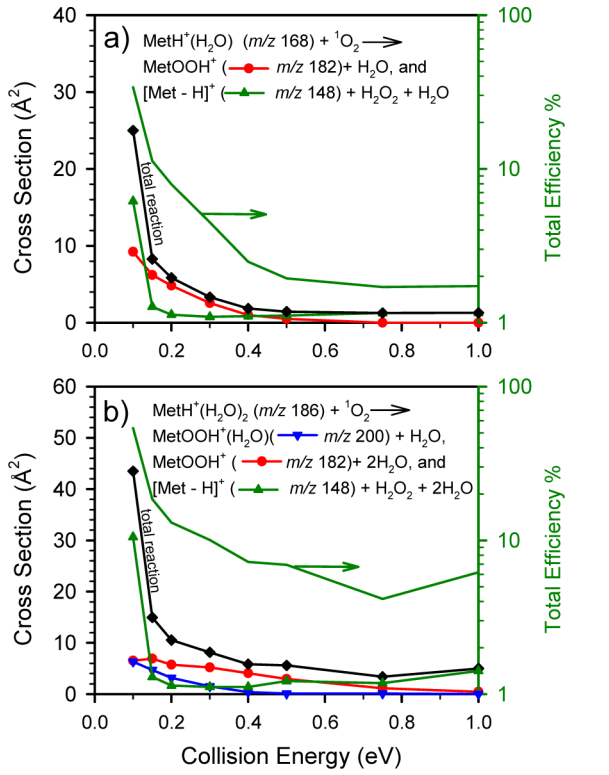

Figure 3. Product cross sections for the reactions of $^1O_2$ with (a) $MetH^+(H_2O)$ and (b) $MetH^+(H_2O)_2$, as a function of E_{col}. Reaction efficiencies (dark green curves) are shown on the right axis using a log scale.

section is 16 Å^2 for m/z 148 and 9 Å^2 for m/z 182 at $E_{col} = 0.1$ eV and drops to 2.1 Å^2 for m/z 148 and 6.2 Å^2 for m/z 182 at 0.15 eV. The H_2O_2 channel has much sharper E_{col} dependence than $MetOOH^+$, becoming negligible at $E_{col} \geq 0.2$ eV. Therefore, $MetOOH^+$ dominates the products at all collision energies except the lowest one.

For $MetH^+(H_2O)_2$ (m/z 186) + $^1O_2$, besides m/z 148 and 182, $^1O_2$-specific products were found at m/z 200, corresponding to formation of monohydrated $MetOOH^+(H_2O)$. Their cross sections and the total reaction efficiency are plotted in Figure 3b. Similar to its monohydrated counterpart, the reaction of $MetH^+(H_2O)_2 + {}^1O_2$ exhibits exothermic behavior, of which the cross sections increase with decreasing E_{col}. Note that at the lowest E_{col}, a trace of signal was observed at m/z 218, corresponding to the survival reaction intermediate $MetOOH^+(H_2O)_2$.

The reactions of $MetH^+(H_2O)_{1,2}$ are significant only at low energies. An interesting finding is that $MetH^+(H_2O)_2$ is more reactive than $MetH^+(H_2O)$. Reaction efficiencies for $MetH^+(H_2O)$ and $MetH^+(H_2O)_2$ are 34% and 54%, respectively, at $E_{col} = 0.1$ eV. Similar results were reported for the reactions of $^1O_2$ with $CysH^+(H_2O)$ versus $CysH^+(H_2O)_2$.[37] Another interesting finding is that compared to its deprotonated counterparts, reaction efficiencies of $MetH^+(H_2O)$ and

DOI: 10.1021/acs.jpcb.5b03779
J. Phys. Chem. B 2015, 119, 8001−8012

$MetH^+(H_2O)_2$ are 15 and 25 times higher (calculated E_{col} = 0.1 eV), respectively.

In addition to $^1O_2$-specific product ions, we have observed CID product ions[58,59] corresponding to elimination of water, ammonia, and methyl from the $MetH^+(H_2O)_{1,2}$ reactant ions. Since these are not relevant to $^1O_2$ chemistry, they are not discussed further.

3.3. Reaction Mechanisms. *A. Nonreactivity of [Met − H]⁻ with $^1O_2$.* An unexpected experimental result is that no oxidation product was observed for dehydrated $[Met - H]^-$. To explore the origin of the nonreactivity of $[Met - H]^-$, we have mapped out the PES associated with its reaction coordinate. We excluded in the PES the intersystem crossing from $^1O_2$ + $^1[Met - H]^-$ to $^3O_2$ + $^3[Met - H]^-$ because excited $^3[Met - H]^-$ predissociates to $NH_2CH(CH_2CH_2S)CO_2^-$ + CH_3. As illustrated in Figure 4, a weakly bound

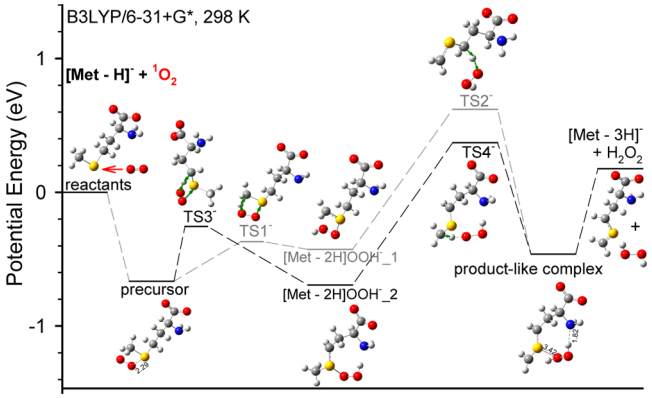

Figure 4. Schematic reaction coordinate for $[Met - H]^-$ + $^1O_2$. Energies of complexes, TSs, and products, relative to reactants, are derived from B3LYP/6-31+G* results, including ZPE. Bond distances are shown in angstroms. For TS, vibrational modes corresponding to the imaginary frequencies are indicated by displacement vectors.

precursor complex and two covalently bound complexes may form during the collision of $[Met - H]^-$ with $^1O_2$. We have located the TSs connecting the complexes to each other and to the products. Two oxidation product channels may be proposed, both of which involve the precursor complex. The precursor complex is formed by electrostatic interaction and has a binding energy of 0.67 eV with respect to reactants. The precursor is rather floppy, with large amplitude of intermolecular motion. It allows repeated encounters between the reactants, increasing the probability of crossing activation barriers to form covalently bound hydroperoxides $[Met - 2H]OOH^-$_1 and 2.

The first product channel follows reactants → precursor complex → $TS1^-$ → $[Met - 2H]OOH^-$_1 → $TS2^-$ → product-like complex → $[Met - 3H]^-$ + H_2O_2. After forming the precursor, an H is transferred from $-SCH_3$ to the O_2 moiety at $TS1^-$, followed by formation of $[Met - 2H]OOH^-$_1 (−0.43 eV with respect to the reactants). $TS1^-$ lies 0.37 eV lower than the reactants, suggesting no activation barriers inhibit formation of $[Met - 2H]OOH^-$_1. Within $[Met - 2H]OOH^-$_1, a second H can be transferred from γ-CH_2 to −OOH at $TS2^-$, resulting in a product-like complex consisting of $NH_2CH(CH_2CH{=}SCH_2)CO_2^-\cdots H_2O_2$. The product-like complex lies 0.46 eV below the reactants, with the H_2O_2 molecule hydrogen bonded to the amino group. Dissociation of the product-like complex gives rise to $[Met - 3H]^-$ + H_2O_2. However, this route can be discounted at low E_{col} because its reaction enthalpy is 0.18 eV endothermic; and more importantly, this channel bears a high barrier of 0.62 eV at $TS2^-$.

Another possible product channel corresponds to reactants → precursor → $TS3^-$ → $[Met - 2H]OOH^-$_2 → $TS4^-$ → product-like complex → $[Met - 3H]^-$ + H_2O_2. In this mechanism, the initial H transfer occurs from γ-CH_2 (i.e., $TS3^-$, 0.26 eV below the reactants). The resulting hydroperoxide $[Met - 2H]OOH^-$_2 is structurally different than $[Met - 2H]OOH^-$_1 and is 0.27 eV more stable. $[Met - 2H]OOH^-$_2 may transfer second H from $-SCH_3$ to −OOH at $TS4^-$, followed by H_2O_2 elimination to yield the $[Met - 3H]^-$ product. We were unable to locate $TS4^-$ using traditional TS searching methods (e.g., TS, QST2, and QST3 in Gaussian 09). The $TS4^-$ barrier height was determined using a relaxed potential energy surface scan running along the hydrogen transfer from $-SCH_3$ to the oxygen terminal of −OOH. The PES scan continuously varied the new bond length rOH from 2.73 to 0.99 Å and optimized all coordinates other than rOH. The PES scan yielded a single barrier associated with hydrogen transfer, with its energy 1.06 eV higher than that of $[Met - 2H]OOH^-$_2. The barrier height is similar to that from $[Met - 2H]OOH^-$_1 to $TS2^-$. Consequently, this channel is also disfavored at low E_{col}.

One may question that, since there are no activation barriers leading to formation of $[Met - 2H]OOH^-$_1 and 2, why neither of these was detected in the experiment. The mechanistic importance of the precursor and hydroperoxide intermediates depends on their lifetimes, so we have used the RRKM theory to calculate the rates for all unimolecular channels leading from these complexes as indicated in the PES. No barrier is expected for decay of the precursor to reactants (i.e., no reaction) in excess of the asymptote, thus an orbiting transition state[60] was assumed. Rotation quantum number K was treated as active in evaluating unimolecular rate constant $k(E, J)$ so that all $(2J + 1)$ K-levels are counted as follows:[61]

$$k(E, J) = \frac{d}{h}\frac{\sum_{K=-J}^{J} G[E - E_0 - E_r^{\dagger}(J, K)]}{\sum_{K=-J}^{J} N[E - E_r(J, K)]}$$

where d is the reaction path degeneracy, G is the sum of states from 0 to $E - E_0 - E_r^{\dagger}$ at the transition state, N is the reactant density of states, E is the system energy, E_0 is the unimolecular dissociation threshold, and E_r and $E_r^{\dagger}$ are the rotational energies for the reactant and the transition state, respectively. The orbital angular momentum L was estimated from $\sigma_{collision}$ [i.e., $L = \mu v_{rel}(\sigma_{collision}/\pi)^{1/2}$], where μ and v_{rel} are the reduced mass and the relative velocity of collision partners, respectively. Complexes and TSs were described using frequencies, polarizabilities, and momenta of inertia obtained from DFT calculations.

Analysis of RRKM results provides kinetic insights. At $E_{col} \leq$ 0.2 eV (where we expect that a complex-mediated mechanism might be important), the dominant decay channel for the precursor complex corresponds to precursor → $TS1^-$ → $[Met - 2H]OOH^-$_1 with a rate constant k of $4–6 \times 10^8$ s^{-1}, followed by precursor → $TS3^-$ → $[Met - 2H]OOH^-$_2 with $k = 1–2 \times 10^7$ s^{-1}, while the k for decay back to reactants is less than 1×10^7 s^{-1}. The dominant channel for both $[Met - 2H]OOH^-$_1 and $[Met - 2H]OOH^-$_2 correspond to "back to the precursor" (because of tight and high $TS2^-$ and $TS4^-$ in the product channels), and their rate constants are 2×10^{11} and

DOI: 10.1021/acs.jpcb.5b03779
J. Phys. Chem. B 2015, 119, 8001−8012

1×10^8 s^{-1}, respectively. Since [Met − 2H]OOH^-_1 has the shortest lifetime compared to others, its mechanistic importance may be doubtful. On the other hand, the lifetimes of the precursor and [Met − 2H]OOH^-_2 are in the right range to mediate a reaction. Both complexes have a lifetime longer than the direct collision time (∼1 ps, the time required for a 10 Å motion of reactants at v_{rel}), and the classical rotational period of these complexes (which is ∼10 ps as estimated using the average angular momentum). Because these two complexes interconvert rapidly during their lifetimes, they should be treated as a single complex. Their total lifetime roughly equals the length of time the system is trapped within the potential wells. In that case, the maximum complex lifetime is determined by how fast the precursor decays back to reactants, which is 0.1 μs at low E_{col}. The ion time-of-flight within the octopole and the second quadrupole is around 10 μs. As a result, these complexes were barely detectable in product mass spectra.

B. [Met − H]$^-$(H$_2$O)$_{1,2}$ + ^{1}O$_2$. As noted, the oxidation pathway of [Met − H]$^-$ moves forward to stable products with the addition of water ligand(s). We first focus on the reaction of [Met − H]$^-$(H$_2$O) with ^{1}O$_2$. The PES for [Met − H]$^-$(H$_2$O) + ^{1}O$_2$ is illustrated in Figure 5. Similar to that for [Met − H]$^-$ + ^{1}O$_2$, a precursor complex and two hydroperoxides may form between [Met − H]$^-$(H$_2$O) and ^{1}O$_2$. Except the additional water ligand, the structures of the complexes and TSs in Figure 5 are similar to those for dry [Met − H]$^-$ in Figure 4. To differentiate the similar species between the dry and hydrated systems, we include a water ligand in the acronyms for hydrated structures [e.g., TS1$^-$(H$_2$O)].

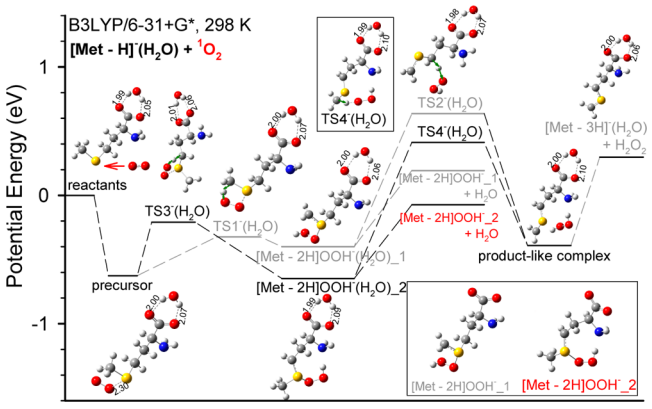

Figure 5. Schematic reaction coordinate for [Met − H]$^-$(H$_2$O) + ^{1}O$_2$. Energies of complexes, TSs, and products, relative to reactants, are derived from B3LYP/6-31+G* results, including ZPE. Bond distances are shown in angstroms.

Two possible pathways which may lead to the observed product of m/z 180 are "reactants → precursor → TS1$^-$(H$_2$O) → [Met − 2H]OOH^-(H$_2$O)_1 → [Met − 2H]OOH^-_1 + H$_2$O", and "reactants → precursor → TS3$^-$(H$_2$O) → [Met − 2H]OOH^-(H$_2$O)_2 → [Met − 2H]OOH^-_2 + H$_2$O". At the early stage of the reaction, [Met − H]$^-$(H$_2$O) follows the same routes as those for [Met − H]$^-$ (see Figure 4), forming hydrated hydroperoxide [Met − 2H]OOH^-(H$_2$O)_1 and 2. Both hydrated hydroperoxides may eliminate the water ligand to [Met − 2H]OOH^-_1 and 2 (m/z 180), respectively. Their DFT-calculated reaction enthalpies are 0.19 and −0.07 eV, respectively. Therefore, [Met − 2H]OOH^-_2 is more energetically favored, and dominates the oxidation product at low E_{col}. While [Met − 2H]OOH^-_1 might be expected at high energies, the E_{col} dependence of product cross section (see Figure 2) suggests its contribution is insignificant.

We have considered the possibility of H$_2$O$_2$ elimination from the hydrated hydroperoxides. This could happen either via [Met − 2H]OOH^-(H$_2$O)_1 → TS2$^-$(H$_2$O) → product-like complex (where a second H is transferred from γ-CH$_2$ to −OOH) or via [Met − 2H]OOH^-(H$_2$O)_2 → TS4$^-$(H$_2$O) → product-like complex (where a second H moves from −SCH$_3$ to −OOH). Both routes end up with a product-like complex which lies 0.39 eV below the reactants and consists of hydrogen-bonded H$_2$O$_2$···[Met − 3H]$^-$···H$_2$O. This complex may expel H$_2$O$_2$ or water or both, with the overall ΔH_{rxn} of 0.30, 0.16, and 0.80 eV, respectively. It is therefore less likely to have these pathways contribute to the reaction at low E_{col}.

A similar mechanism can be proposed for the reaction of dihydrated [Met − H]$^-$(H$_2$O)$_2$ + ^{1}O$_2$. Reaction enthalpies for possible product channels are listed below, all of which have no activation barriers above the reactants. On the basis of the calculated ΔH_{rxn} values, the favored products at low E_{col} belongs to [Met − 2H]OOH^-(H$_2$O)_2.

$$[\text{Met - H}]^-(H_2O)_2 + {}^1O_2 \rightarrow \quad [\text{Met - 2H}]OOH^-(H_2O)\_1 + H_2O \quad \Delta H_{rxn} = 0.08 \text{ eV} \quad (1a)$$

$$[\text{Met - 2H}]OOH^-(H_2O)\_2 + H_2O \quad \Delta H_{rxn} = -0.16 \text{ eV} \quad (1b)$$

$$[\text{Met - 2H}]OOH^-\_1 + 2H_2O \quad \Delta H_{rxn} = 0.67 \text{ eV} \quad (1c)$$

$$[\text{Met - 2H}]OOH^-\_2 + 2H_2O \quad \Delta H_{rxn} = 0.41 \text{ eV} \quad (1d)$$

C. MetH$^+$(H$_2$O)$_{1,2}$ + ^{1}O$_2$. Among the conformations of MetH$^+$(H$_2$O) presented in Figure 1, MetH$^+$(H$_2$O)_1 and 2 are predicted to have a population of 52% and 33%, respectively. On the basis of the significance of their populations, we have considered both conformers in the reaction mechanism. To differentiate the water binding sites in MetH$^+$(H$_2$O)_1 and 2, we include the termini to which water binds in the formulas [i.e., MetH$^+$(H$_2$O)_1 is referred to as MetH$^+$(N-H$_2$O), and MetH$^+$(H$_2$O)_2 as MetH$^+$(C-H$_2$O) in the PESs and discussion]. For dihydrated MetH$^+$, we used MetH$^+$(H$_2$O)$_2$_1 as the reactant structure.

We have reported a reaction mechanism for dehydrated MetH$^+$ + ^{1}O$_2$,[29] which involves formation of hydroperoxide intermediate MetOOH$^+$ and its dissociation to [Met − H]$^+$ and H$_2$O$_2$. Considering the similarities between the chemistry and the products of MetH$^+$ and its hydrates, we may reasonably presume that the products of m/z 148, 182, and 200 observed in the reactions of MetH$^+$(H$_2$O)$_{1,2}$ + ^{1}O$_2$ correspond to the formation of [Met − H]$^+$, MetOOH$^+$, and MetOOH$^+$(H$_2$O), respectively. Their structures are shown in Figures 6 and 7, and the reaction enthalpies calculated at B3LYP/6-31+G(d) are summarized as follows:

DOI: 10.1021/acs.jpcb.5b03779
J. Phys. Chem. B 2015, 119, 8001−8012

$MetH^+(N\text{-}H_2O) + {}^1O_2$

→ $MetOOH^+\_1/MetOOH^+\_2 + H_2O$ ΔH_{rxn}= -0.35/-0.52 eV (2a/b)

→ $H_2NCH(CO_2H)C_2H_4S^+{=}CH_2$ (P1) + H_2O_2 + H_2O ΔH_{rxn} = 0.08 eV (2c)

→ five-membered *cyclic*-$[HNCH(CO_2H)C_2H_4S(CH_3)]^+$ (P2) + H_2O_2 + H_2O ΔH_{rxn} = -0.29 eV (2d)

→ six-membered *cyclic*-$[H_2NCH(CO_2H)C_2H_4SCH_2]^+$ (P3) + H_2O_2 + H_2O ΔH_{rxn} = -1.00 eV (2e)

$MetH^+(C\text{-}H_2O) + {}^1O_2$

→ $MetOOH^+\_1/MetOOH^+\_2 + H_2O$ ΔH_{rxn}= -0.37/-0.54 eV (2a'/b')

→ $H_2NCH(CO_2H)C_2H_4S^+{=}CH_2$ (P1) + H_2O_2 + H_2O ΔH_{rxn} = 0.06 eV (2c')

→ five-membered *cyclic*-$[HNCH(CO_2H)C_2H_4S(CH_3)]^+$ (P2) + H_2O_2 + H_2O ΔH_{rxn} = -0.31 eV (2d')

→ six-membered cyclic-$[H_2NCH(CO_2H)C_2H_4SCH_2]^+$ (P3) + H_2O_2 + H_2O ΔH_{rxn} = -1.02 eV (2e')

$MetH^+(H_2O)_2 + {}^1O_2$

→ $MetOOH^+(N\text{-}H_2O)\_1 + H_2O$ ΔH_{rxn}= -0.20 eV (3a)

→ $MetOOH^+(C\text{-}H_2O)\_1 + H_2O$ ΔH_{rxn} = -0.33 eV (3b)

→ $MetOOH^+(N\text{-}H_2O)\_2 + H_2O$ ΔH_{rxn} = -0.37 eV (3c)

→ $MetOOH^+(C\text{-}H_2O)\_2 + H_2O$ ΔH_{rxn} = -0.48 eV (3d)

→ $MetOOH^+\_1 + 2H_2O$ ΔH_{rxn} = 0.24 eV (3e)

→ $MetOOH^+\_2 + 2H_2O$ ΔH_{rxn} = 0.07 eV (3f)

→ $H_2NCH(CO_2H)C_2H_4S^+{=}CH_2$ (P1) + H_2O_2 + $2H_2O$ ΔH_{rxn} = 0.69 eV (3g)

→ five-membered *cyclic*-$[HNCH(CO_2H)C_2H_4S(CH_3)]^+$ (P2) + H_2O_2 + $2H_2O$ ΔH_{rxn} = 0.38 eV (3h)

→ six-membered *cyclic*-$[H_2NCH(CO_2H)C_2H_4SCH_2]^+$ (P3) + H_2O_2 + $2H_2O$ ΔH_{rxn} = -0.28 eV (3i)

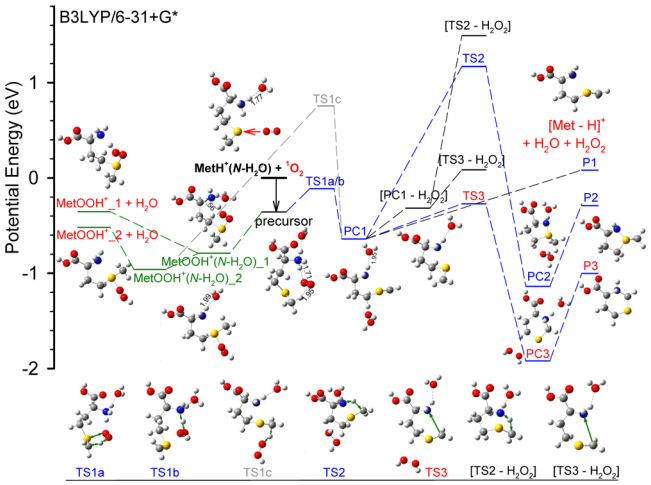

Figure 6. Schematic reaction coordinate for $MetH^+(N\text{-}H_2O)$ + $^1O_2$. Energies of complexes, TSs, and products, relative to reactants, are derived from B3LYP/6-31+G* results, including ZPE. Bond distances are shown in angstroms.

The PES associated with the low-energy pathways for $MetH^+(N\text{-}H_2O)$ + $^1O_2$ is summarized in Figure 6, with the reactants shown near the center at zero energy. $MetH^+(C\text{-}H_2O)$ follows identical reaction pathway as $MetH^+(N\text{-}H_2O)$. $MetH^+(N\text{-}H_2O)$ may form a precursor complex with $^1O_2$, with O_2 sandwiched between the ammonium group and the $-SCH_3$ group. Its binding energy is 0.36 eV. The precursor interconverts to a covalently bound complex $MetOOH^+(N\text{-}H_2O)\_1$, of which one proton is transferred from the ammonium group to the $-SOO$ group, leading to an eight-membered ring with strong hydrogen bonding. $MetOOH^+(N\text{-}H_2O)\_2$ is an analogue of $MetOOH^+(N\text{-}H_2O)\_1$, except that the hydroperoxide group of $MetOOH^+(N\text{-}H_2O)\_2$ swings away from the amino group. The energy of $MetOOH^+(N\text{-}H_2O)\_2$ (−0.96 eV) is slightly lower than that of

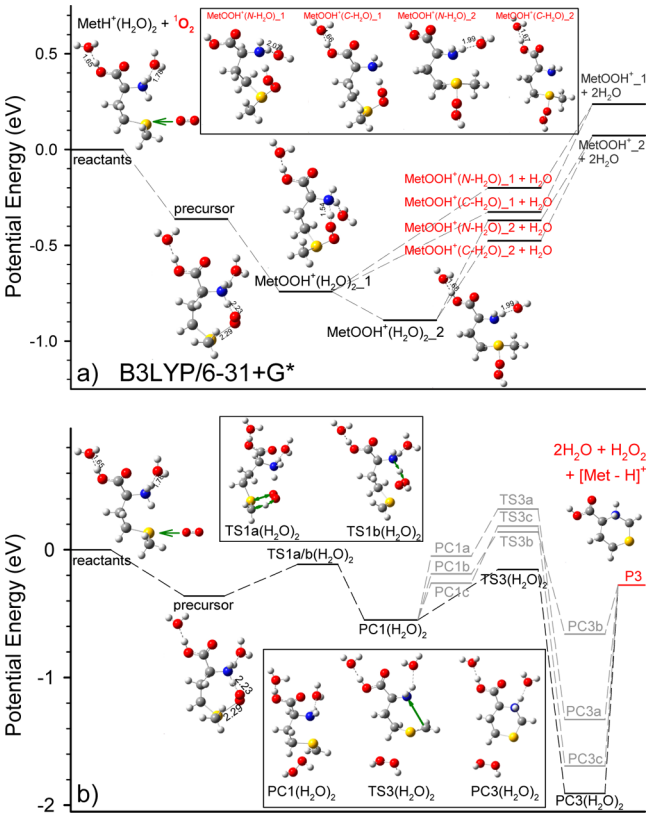

Figure 7. Schematic reaction coordinate for $MetH^+(H_2O)_2$ + $^1O_2$. (a) Formation of hydroperoxides and (b) H_2O_2 elimination. Energies of complexes, TSs, and products, relative to reactants, are derived from B3LYP/631+G* results, including ZPE. Bond distances are shown angstroms. PC1a/b/c, TS3a/b/c, and PC3a/b/c represent the remaining structures of $PC1(H_2O)_2$, $TS3(H_2O)_2$, and $PC3(H_2O)_2$ after eliminating $N\text{-}H_2O$, $C\text{-}H_2O$, and H_2O_2, respectively.

$MetOOH^+(N\text{-}H_2O)\_1$ (−0.79 eV), presumably because of the strong S−N interaction in $MetOOH^+(N\text{-}H_2O)\_2$. Both $MetOOH^+(N\text{-}H_2O)\_1$ and 2 may eliminate the water molecule to form the product ions $MetOOH^+\_1$ and 2 (m/z 182), respectively.

An energetically feasible pathway to the product ion of m/z 148 is depicted in Figure 6 as reactants → precursor → TS1a → TS1b → PC1 → TS3 → PC3 → P3. Instead of forming hydroperoxides, this pathway eliminates H_2O_2 from the precursor via two consecutive activation barriers TS1a and TS1b. At TS1a the O_2 abstracts an H atom from $-SCH_3$, followed by the second H from the ammonium group at TS1b. TS1a and TS1b are located 0.11 and 0.58 eV below the reactants, respectively. Both H_2O_2 and H_2O are hydrogen bonded in the ensuing product-like intermediate PC1 (−0.64 eV). PC1 may cross TS3 (0.27 eV below the reactants) to another product-like complex PC3 (−1.92 eV), where a covalent bond is formed between $-NH_2$ and the terminal $-CH_2$, yielding a six-membered heterocyclic compound hydrogen-bonded with H_2O_2 and H_2O. The subsequent elimination of H_2O_2 and H_2O from PC3 yields six-membered heterocyclic product ion P3.

It is not unreasonable to assume that elimination of H_2O_2 and H_2O may take place at PC1 to yield product ion P1 (i.e., $H_2NCH(CO_2H)CH_2CH_2SCH_2^+$, m/z 148). However, this pathway is not the most favorable at low E_{col} due to the associated 0.08 eV endothermicity. Another possible inter-

DOI: 10.1021/acs.jpcb.5b03779
J. Phys. Chem. B 2015, 119, 8001−8012

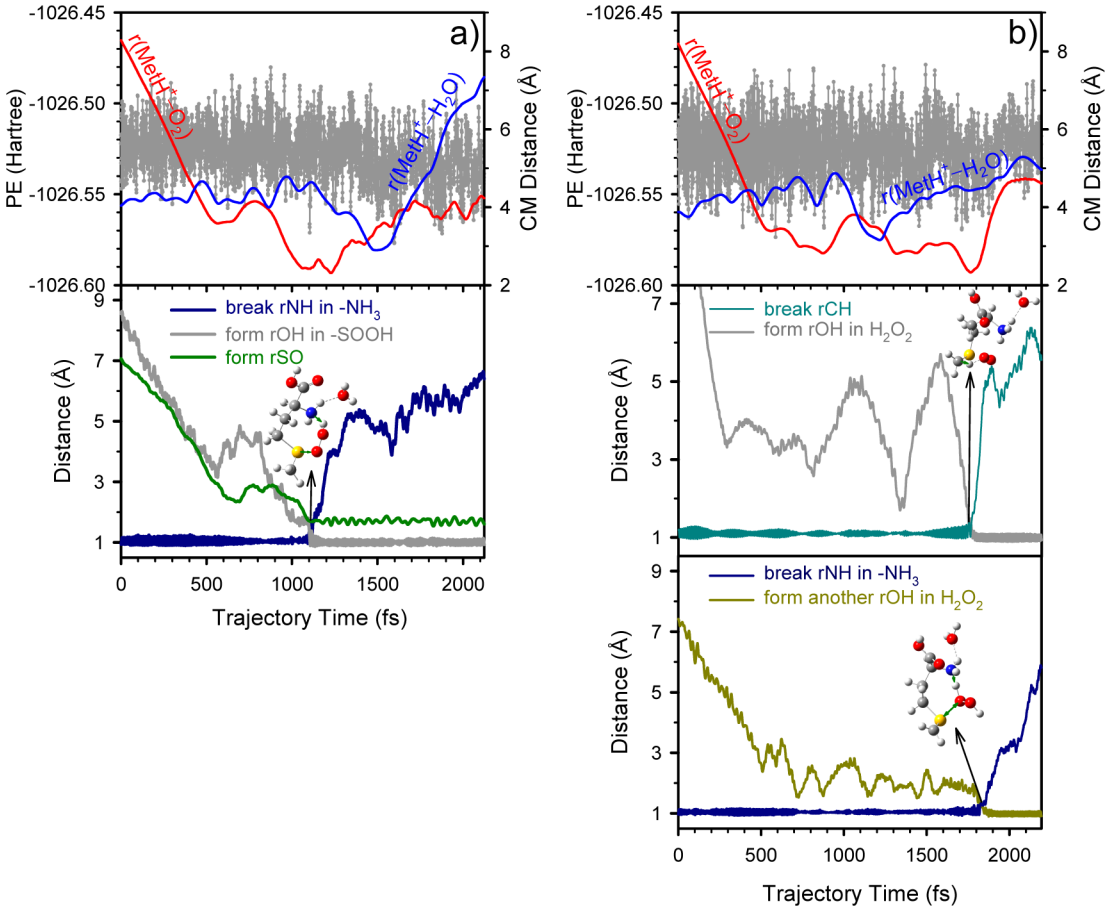

Figure 8. Representative plots of (a) a hydroperoxide-forming trajectory and (b) an H_2O_2-eliminating trajectory for $MetH^+(N\text{-}H_2O) + {}^1O_2$.

conversion of PC1 is to transfer a hydrogen from $-NH_2$ to the terminal $-CH_2$ (i.e., TS2) followed by ring closure to form a five-membered heterocyclic complex PC2 (−1.14 eV), which ultimately dissociates to product ion P2. The overall reaction enthalpy for the path "reactants → precursor → TS1a/b → PC1 → TS2 → PC2 → P2 + H_2O_2 + H_2O" is −0.29 eV. However, the associated barrier TS2 (1.17 eV) makes this process impossible in our E_{col} range.

The proposed mechanism for hydrated $MetH^+$ raises a question if elimination of water could happen at any time of the reaction. A related question is to what extent the existence of water affects reaction progress; more specifically, whether it is necessary to retain the water ligand until the last step of the reaction. We could image two scenarios for the PES of Figure 6. In the first scenario, departure of water takes place at the very early stage, subsequent to formation of the precursor. Since the precursor binding energy is much less than the $MetH^+$ hydration energy, water elimination from the precursor is endothermic. It follows that both the $MetOOH^+$ formation and the H_2O_2 elimination channels would shut down at low E_{col}. In the second scenario, water leaves from PC1. The remaining dehydrated PC1 only has the H_2O_2 moiety hydrogen bonded and lies −0.26 eV below the reactants (0.38 eV higher than the original PC1). In this case, all the barriers following PC1 would be lifted by 0.31−0.49 eV, and all the downstream pathways become endothermic. Both scenarios make the reaction pathways energetically much less favorable, implying the mechanistic importance of water along the reaction course. This also implies the potential protection against Met oxidative damage by water elimination in biological systems.

We have calculated the possibility of eliminating H_2O_2 only at PC1, labeled as [PC1 − H_2O_2] (a hydrated analogue of P1). [PC1 − H_2O_2] can either form a five-member ring at [TS2 − H_2O_2] or a six-member ring at [TS3 − H_2O_2]. But [TS2 − H_2O_2] and [TS3 − H_2O_2] lie at even higher energies (1.49 and 0.1 eV) than TS2 and TS3, respectively.

Computation results for the reaction of $MetH^+(H_2O)_2 + {}^1O_2$ are summarized in Figure 7. We split the PES into two frames. The portion of PES corresponding to formation of hydroperoxides are shown in Figure 7a [i.e., reactants → precursor → $MetOOH^+(H_2O)_2\_1$ → $MetOOH^+(C\text{-}H_2O)\_1$/$MetOOH^+(N\text{-}H_2O)\_1$ (m/z 200) + H_2O]. $MetOOH^+(H_2O)_2\_1$ may interconvert to $MetOOH^+(H_2O)_2\_2$, followed by water elimination to $MetOOH^+(C\text{-}H_2O)\_2$/$MetOOH^+(N\text{-}H_2O)\_2$ (m/z 200). $MetOOH^+(N\text{-}H_2O)\_1$ and 2 and $MetOOH^+(C\text{-}H_2O)\_1$ and 2 may undergo further water dissociation, yielding bare $MetOOH^+\_1$ and 2 (m/z 182). All single-water elimination channels (eqs 3a−3d) are exothermic, and one of the double-water elimination channels (i.e., eq 3f) is nearly thermal; therefore, both single- and double-water elimination were observed in the hydroperoxide products.

As calculated in eqs 3g−3i, only the product channel of six-membered *cyclic*-$[H_2NCH(CO_2H)C_2H_4SCH_2]^+$ (P3) + H_2O_2 + $2H_2O$ (eq 3i) may account for the product ion of m/z 148 at low E_{col}. This route is depicted in Figure 7b, of which the involved intermediates and TSs are dihydrated analogues to those for $MetH^+(H_2O) + {}^1O_2$. The reaction follows reactants

DOI: 10.1021/acs.jpcb.5b03779
J. Phys. Chem. B 2015, 119, 8001−8012

→ precursor (−0.36 eV) → TS1a$(H_2O)_2$ (−0.11 eV) → TS1b$(H_2O)_2$ (−0.52 eV) → PC1$(H_2O)_2$ (−0.55 eV) → TS3$(H_2O)_2$ (−0.15 eV) → PC3$(H_2O)_2$ (−1.91 eV) → P3 + H_2O_2 + $2H_2O$. To achieve favorable reaction energetics, the two water molecules and the H_2O_2 have to be all retained in TS3$(H_2O)_2$; the dissociation of *N*-H_2O, *C*-H_2O, or H_2O_2 would increase this activation barrier by 0.47 (labeled as TS3a in the PES), 0.29 (TS3b), and 0.34 eV (TS3c), respectively. The resulting pathways are illustrated by dark gray lines in Figure 7b, all of which are disfavored in our E_{col} range.

3.4. Dynamics Simulations of MetH$^+$(*N*-H_2O) + $^1O_2$. A further understanding of the collision dynamics for MetH$^+$(*N*-H_2O) + $^1O_2$ was obtained by examining their trajectories at E_{col} = 0.1 and 0.2 eV. Two hundred trajectories were completed at each E_{col}. All trajectories were calculated at b = 0.1 Å using B3LYP/4−31G(d). While some trajectories completed reactions within trajectory simulation times (2−3 ps), a large fraction of the trajectories either remained as complex or belong to nonreactive collisions (i.e., fly by without forming long-lasting complexes). We exemplify three trajectories in Figures 8 and 9, all of which were obtained at E_{col} = 0.1 eV.

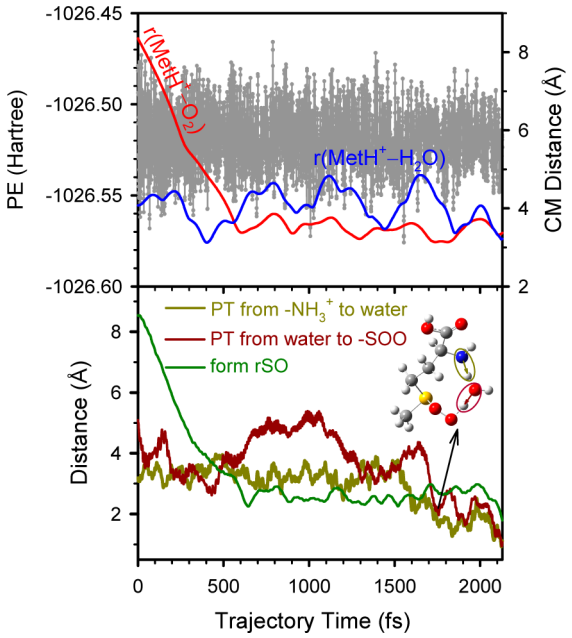

Figure 9. A trajectory shows water-assisted proton transfer (indicated by two ellipses) in formation of hydroperoxide from MetH$^+$(*N*-H_2O) + $^1O_2$.

A trajectory producing MetOOH$^+$ and a separated water molecule is depicted in Figure 8a. The top frame shows the change in the potential energy (PE), the approaching of reactants and the separation of products [as indicated by the center-of-masses distances r(MetH$^+$-O_2) and r(MetH$^+$- H_2O)] during the trajectory. The bottom frame shows formation of the S−O bond as indicated by the decrease of *r*SO at ∼1060 fs. At ∼ 1120 fs, an H is transferred from $-NH_3$ to −SOO, as indicated by the changes of *r*NH and *r*OH. High-frequency oscillations of various bonds reflect the vibrations of the reactants or products. This trajectory verifies the reaction pathway proposed in Figure 6. Elimination of water occurs after completion of proton transfer. By the end of the trajectory, water is separated from MetOOH$^+$ by 7.3 Å.

Figure 8b illustrates a trajectory that eliminates H_2O_2 and H_2O. At 1750 fs, an H is transferred from $-SCH_3$ to one end of the O_2 (see middle frame), followed by transfer of a second H from $-NH_3$ to the other end of O_2 and subsequent elimination of H_2O_2 at 1810 fs (see bottom frame). The bonds plotted in Figure 8b correspond to the breakage of rCH in $-SCH_3$ and rNH in $-NH_3$, formation of two rOH bonds in H_2O_2, and the S−O interaction during the trajectory.

Trajectory simulations show that all of the persulfoxides and hydroperoxides formed in the trajectories did not decay back to reactants before the termination of the trajectories. This indicates that the lifetimes of these complexes are at least no less than the trajectory time (typically 2−3 ps), and therefore, they are mechanistically important.

4. SUMMARY

4.1. Kinetic Influences of Microsolvation. Hydroperoxide intermediates were formed in the reactions of $^1O_2$ with both protonated and deprotonated Met as verified by PES calculations and trajectory simulations; however, none of these hydroperoxides were stable enough to be observed as end-products. In the reaction of MetH$^+$ + $^1O_2$, MetOOH$^+$ facilitates the intramolecular H transfer from MetH$^+$ to O_2, and an H_2O_2 elimination channel was observed as a result. In the reaction of [Met − H]$^-$ + $^1O_2$, [Met − 2H]OOH $^-$ ultimately decayed back to reactants.

In contrast to dry Met ions, hydroperoxides were detected as stable products in the $^1O_2$ oxidation of hydrated Met (in both ionization states). The key to understand these phenomena is that a microsolvation environment provides these hydroperoxides a mechanism by which the energized hydroperoxides can dispose of sufficient internal excitation via water elimination, so that the hydroperoxide moiety does not undergo decomposition. The water dissociation energy is 0.57 eV for [Met − 2H]OOH$^-$(H_2O) and 0.44 eV for MetOOH$^+$(H_2O). This energy can be compensated by the reaction enthalpy gained from the formation of hydroperoxides. In this sense, even a single water ligand can have a big impact on dynamics. Since no activation barrier would be expected for water elimination, formation of MetOOH$^+$ products is generally favored than H_2O_2 elimination in the reactions of MetH$^+$$(H_2O)_{1-2}$.

As noted, MetH$^+$$(H_2O)_2$ has a higher reaction efficiency than MetH$^+$(H_2O). This could be due to two factors. First, density of vibrational states in the dihydrated system is higher than that in the monohydrated system, and so the intramolecular vibrational relaxation is faster for prompt dissociation of water. Second, the second water ligand is less strongly bonded to MetH$^+$ than the first one, and thus is easier to dissociate. Interestingly, the second water has little effect on the reaction efficiency of deprotonated Met. In addition, hydrated MetH$^+$ is much more reactive toward $^1O_2$ compared to hydrated [Met-H]$^-$, mostly because the interconversion from precursor to the key intermediate hydroperoxide is barrierless in the protonated systems, but this is not the case in the deprotonated ones.

A complication in thinking about the reactions of hydrated clusters with $^1O_2$ is that the water ligands may physically quench $^1O_2$ during collisions. In the present experiment, we were not able to directly probe the physical quenching of $^1O_2$. The quasi-classical trajectory method cannot simulate the physical quenching of $^1O_2$, either. However, trajectory simulations illustrate that at E_{col} = 0.1 and 0.2 eV, only less than 8% and 18% of collisions have $^1O_2$ attack the water ligand

DOI: 10.1021/acs.jpcb.5b03779
J. Phys. Chem. B 2015, 119, 8001−8012

of $MetH^+(H_2O)$ directly. Only a fraction of such collisions may actually quench $^1O_2$. Therefore, it is less likely that the physical quenching by water would significantly affect the branching of $^1O_2$ chemical reactions.

4.2. Dynamical Role of Water. The above scheme may lead to an impression that the water in hydrated Met clusters acts like a spectator such as rare gas tagging and represents very weak perturbations to host dynamics.[62−64] However, this is not true for the oxidation of hydrated Met. A trajectory showing water-catalyzed proton transfer for $MetH^+(N\text{-}H_2O)$ + $^1O_2$ is demonstrated in Figure 9. This trajectory undergoes concerted transfer of two protons at ∼1700 fs; one proton is transferred from $-NH_3$ to water and simultaneously another from water to −SOO. At the same time, a persulfoxide bond is formed between the O_2 moiety and S, leading to $MetOOH^+(H_2O)$. Water is intimately involved in Met oxidation, and the reaction coordinate is altered by the absorbed water.

■ ASSOCIATED CONTENT

Supporting Information

Cartesian coordinates for stable conformers of $[Met - H]^-$, $[Met - H]^-(H_2O)$, $[Met - H]^-(H_2O)_2$, $MetH^+(H_2O)$, and $MetH^+(H_2O)_2$. The Supporting Information is available free of charge on the ACS Publications website at DOI: 10.1021/acs.jpcb.5b03779.

■ AUTHOR INFORMATION

Corresponding Author

*E-mail: jianbo.liu@qc.cuny.edu. Tel: 1-718-997-3271.

Notes

The authors declare no competing financial interest.

■ ACKNOWLEDGMENTS

This work was supported by the National Science Foundation CAREER Award (Grant CHE-0954507), Queens College Research Enhancement Funds and PSC−CUNY Research Awards.

■ REFERENCES

(1) Ogilby, P. R. Singlet Oxygen: There Is Indeed Something New under the Sun. *Chem. Soc. Rev.* **2010**, *39*, 3181−3209.

(2) Foote, C. S. Mechanisms of Photosensitized Oxidation. *Science* **1968**, *162*, 963−970.

(3) Davies, M. J. Singlet Oxygen-Mediated Damage to Proteins and Its Consequences. *Biochem. Biophys. Res. Commun.* **2003**, *305*, 761−770.

(4) Davies, M. J. Reactive Species Formed on Proteins Exposed to Singlet Oxygen. *Photochem. Photobiol. Sci.* **2004**, *3*, 17−25.

(5) Davies, M. J. The Oxidative Environment and Protein Damage. *Biochim. Biophys. Acta* **2005**, *1703*, 93−109.

(6) Sysak, P. K.; Foote, C. S.; Ching, T.-Y. Chemistry of Singlet Oxygen. XXV. Photooxygenation of Methionine. *Photochem. Photobiol.* **1977**, *26*, 19−27.

(7) Valley, C. C.; Cembran, A.; Perlmutter, J. D.; Lewis, A. K.; Labello, N. P.; Gao, J.; Sachs, J. N. The Methionine-Aromatic Motif Plays a Unique Role in Stabilizing Protein Structure. *J. Biol. Chem.* **2012**, *287*, 34979−34991.

(8) Lavine, T. F. Formation, Resolution, and Optical Properties of the Diastereoisomeric Sulfoxides Derived from L-Methionine. *J. Biol. Chem.* **1947**, *169*, 477−91.

(9) Vogt, W. Oxidation of Methionyl Residues in Proteins: Tools, Targets, and Reversal. *Free Radicals Biol. Med.* **1995**, *18*, 93−105.

(10) Chao, C.-C.; Ma, Y.-S.; Stadtman, E. R. Modification of Protein Surface Hydrophobicity and Methionine Oxidation by Oxidative Systems. *Proc. Natl. Acad. Sci. U.S.A.* **1997**, *94*, 2969−2974.

(11) Brot, N.; Weissbach, L.; Werth, J.; Weissbach, H. Enzymic Reduction of Protein-Bound Methionine Sulfoxide. *Proc. Natl. Acad. Sci. U.S.A.* **1981**, *78*, 2155−8.

(12) Caldwell, P.; Luk, D. C.; Weissbach, H.; Brot, N. Oxidation of the Methionine Residues of Escherichia Coli Ribosomal Protein L12 Decreases the Protein's Biological Activity. *Proc. Natl. Acad. Sci. U.S.A.* **1978**, *75*, 5349−52.

(13) Sacksteder, C. A.; Whittier, J. E.; Xiong, Y.; Li, J.; Galeva, N. A.; Jacoby, M. E.; Purvine, S. O.; Williams, T. D.; Rechsteiner, M. C.; Bigelow, D. J.; Squier, T. C. Tertiary Structural Rearrangements Upon Oxidation of Methionine145 in Calmodulin Promotes Targeted Proteasomal Degradation. *Biophys. J.* **2006**, *91*, 1480−1493.

(14) Stadtman, E. R.; Remmen, H. V.; Richardson, A.; Wehr, N. B.; Levine, R. L. Methionine Oxidation and Aging. *Biochim. Biophys. Acta* **2005**, *1703*, 135−140.

(15) Glaser, C.; Schoeneich, C. *Special Issue: Methionine Oxidation and Methionine Sulfoxide Reductases. [In: Biochim. Biophys. Acta; 2005, 1703(2)]*; Elsevier B.V.: Amsterdam, Netherlands, 2005.

(16) Brot, N.; Weissbach, H. Biochemistry and Physiological Role of Methionine Sulfoxide Residues in Proteins. *Arch. Biochem. Biophys.* **1983**, *223*, 271−81.

(17) Grimaud, R.; Ezraty, B.; Mitchell, J. K.; Lafitte, D.; Briand, C.; Derrick, P. J.; Barras, F. Repair of Oxidized Proteins: Identification of a New Methionine Sulfoxide Reductase. *J. Biol. Chem.* **2001**, *276*, 48915−48920.

(18) Delaye, L.; Becerra, A.; Orgel, L.; Lazcano, A. Molecular Evolution of Peptide Methionine Sulfoxide Reductases (Msra and Msrb): On the Early Development of a Mechanism That Protects against Oxidative Damage. *J. Mol. Evol.* **2007**, *64*, 15−32.

(19) Garner, B.; Waldeck, A. R.; Witting, P. K.; Rye, K.-A.; Stocker, R. Oxidation of High Density Lipoproteins II. Evidence for Direct Reduction of Lipid Hydroperoxides by Methionine Residues of Apolipoproteins Ai and Aii. *J. Biol. Chem.* **1998**, *273*, 6088−6095.

(20) Levine, R. L.; Mosoni, L.; Berlett, B. S.; Stadtman, E. R. Methionine Residues as Endogenous Antioxidants in Proteins. *Proc. Natl. Acad. Sci. U.S.A.* **1996**, *93*, 15036−15040.

(21) Weil, L.; Gordon, W. G.; Buchert, A. R. Photooxidation of Amino Acids in the Presence of Methylene Blue. *Arch. Biochem.* **1951**, *33*, 90−109.

(22) Spikes, J. D.; MacKnight, M. L. Dye-Sensitized Photooxidation of Proteins. *Ann. N.Y. Acad. Sci.* **1970**, *171*, 149−162.

(23) Cohen, S. G.; Ojanpera, S. Photooxidation of Methionine and Related Compounds. *J. Am. Chem. Soc.* **1975**, *97*, 5633−5634.

(24) Rougee, M.; Bensasson, R. V.; Land, E. J.; Pariente, R. Deactivation of Singlet Molecular Oxygen by Thiols and Related Compounds, Possible Protectors against Skin Photosensitivity. *Photochem. Photobiol.* **1988**, *47*, 485−9.

(25) Bertolotti, S. G.; Garcia, N. A.; Arguello, G. A. Effects of the Peptide Bond on the Singlet-Molecular-Oxygen-Mediated Sensitized Photo-Oxidation of Tyrosine and Tryptophan Dipeptides. A Kinetic Study. *J. Photochem. Photobiol., B* **1991**, *10*, 57−70.

(26) Stadtman, E. R.; Berlett, B. S. Free-Radical-Mediated Modification of Proteins. In *Free Radical Toxicology*; Wallace, K. B., Ed.; Taylor & Francis: Washington, DC, 1997; pp 71−87.

(27) Frimer, A. A. *Singlet O2, Vol III, Reaction Modes and Products, Part 2*; CRC Press: Boca Raton, FL, 1985.

(28) Palumbo, G. Photodynamic Therapy and Cancer: A Brief Sightseeing Tour. *Expert Opin. Drug Delivery* **2007**, *4*, 131−148.

(29) Fang, Y.; Liu, F.; Bennett, A.; Ara, S.; Liu, J. Experimental and Trajectory Study on Reaction of Protonated Methionine with Electronically Excited Singlet Molecular Oxygen ($a^1\Delta_g$): Reaction Dynamics and Collision Energy Effects. *J. Phys. Chem. B* **2011**, *115*, 2671−2682.

(30) Liu, D.; Wyttenbach, T.; Bowers, M. T. Hydration of Protonated Primary Amines: Effects of Intermolecular and Intramolecular Hydrogen Bonds. *Int. J. Mass Spectrom.* **2004**, *236*, 81−90.

DOI: 10.1021/acs.jpcb.5b03779
J. Phys. Chem. B 2015, 119, 8001−8012

(31) Otto, R.; Brox, J.; Trippel, S.; Stei, M.; Best, T.; Wester, R. Single Solvent Molecules Can Affect the Dynamics of Substitution Reactions. *Nat. Chem.* **2012**, *4*.
(32) Wang, X.-B.; Yang, X.; Wang, L.-S. Probing Solution-Phase Species and Chemistry in the Gas Phase. *Int. Rev. Phys. Chem.* **2002**, *21*, 473−498.
(33) Liu, F.; Lu, W.; Fang, Y.; Liu, J. Evolution of Oxidation Dynamics of Histidine: Non-Reactivity in the Gas Phase, Peroxides in Hydrated Clusters and Ph Dependecne in Solution. *Phem. Chem. Chem. Phys.* **2014**, *16*, 22179−22191.
(34) Matheson, I. B. C.; He, J. Chemical Reaction Rates of Amino Acids with Singlet Oxygen. *Photochem. Photobiol.* **1979**, *29*, 879−881.
(35) Liu, F.; Fang, Y.; Chen, Y.; Liu, J. Dissociative Excitation Energy Transfer in the Reactions of Protonated Cysteine and Tryptophan with Electronically Excited Singlet Molecular Oxygen ($a^1\Delta_g$). *J. Phys. Chem. B* **2011**, *115*, 9898−9909.
(36) Fang, Y.; Liu, F.; Emre, R.; Liu, J. Guided-Ion-Beam Scattering and Direct Dynamcis Trajectroy Study on the Reaction of Deprotonated Cysteine with Singlet Molecualar Oxygen. *J. Phys. Chem. B* **2013**, *117*, 2878−2887.
(37) Liu, F.; Emre, R.; Lu, W.; Liu, J. Oxidation of Gas-Phase Hydrated Protonated/Deprotonated Cysteine: How Many Water Ligands Are Sufficient to Approach Solution-Phase Photooxidation Chemistry? *Phys. Chem. Chem. Phys.* **2013**, *15*, 20496−20509.
(38) Fang, Y.; Liu, J. Reaction of Protonated Tyrosine with Electronically Excited Singlet Molecular Oxygen ($a^1\Delta_g$): An Experimental and Trajectory Study. *J. Phys. Chem. A* **2009**, *113*, 11250−11261.
(39) Midey, A.; Dotan, I.; Viggiano, A. A. Temperature Dependences for the Reactions of O^- and O_2^- with $O_2(a^1\Delta_g)$ from 200 to 700 K. *J. Phys. Chem. A* **2008**, *112*, 3040−3045.
(40) Lafferty, W. J.; Solodov, A. M.; Lugez, C. L.; Fraser, G. T. Rotational Line Strengths and Self-Pressure-Broadening Coefficients for the 1.27 μm, $a^1\Delta_g$-$X^3\Sigma_g^-$, V=0−0 Band of O_2. *Appl. Opt.* **1998**, *37*, 2264−2270.
(41) Liu, F.; Fang, Y.; Chen, Y.; Liu, J. Reactions of Deprotonated Tyrosine and Tryptophan with Electronically Excited Singlet Moleuclar Oxygen ($a^1\Delta_g$): A Guided-Ion-Beam Scattering, Statistical Modeling, and Trajectroy Study. *J. Phys. Chem. B* **2012**, *116*, 6369−6379.
(42) Frisch, M. J.; Trucks, G. W.; Schlegel, H. B.; Scuseria, G. E.; Robb, M. A.; Cheeseman, J. R.; Scalmani, G.; Barone, V.; Mennucci, B.; Petersson, G. A.; et al. *Gaussian 09*, revision D.01; Gaussian, Inc: Wallingford, CT, 2013.
(43) Alecu, I. M.; Zheng, J.; Zhao, Y.; Truhlar, D. G. Computational Thermochemistry: Scale Factor Databases and Scale Factors for Vibrational Requencies Obtained from Electronic Model Chemistries. *J. Chem. Theory Comput.* **2010**, *6*, 2872−2887.
(44) Marcus, R. A. Unimolecular Dissociations and Free-Radical Recombination Reactions. *J. Chem. Phys.* **1952**, *20*, 359−364.
(45) Zhu, L.; Hase, W. L. *A General Rrkm Program(QCPE 644), Quantum Chemistry Program Exchange*; Chemistry Department, University of Indiana: Bloomington, 1993.
(46) Hase, W. L.; Bolton, K.; de Sainte Claire, P.; Duchovic, R. J.; Hu, X.; Komornicki, A.; Li, G.; Lim, K.; Lu, D.; Peslherbe, G. H.; et al. *Venus 99: A General Chemical Dynamics Computer Program*; Texas Tech Univeristy: Lubbock, TX, 1999.
(47) Peslherbe, G. H.; Wang, H.; Hase, W. L. Monte Carlo Sampling for Classical Trajectory Simulations. *Adv. Chem. Phys.* **1999**, *105*, 177−201.
(48) Bakken, V.; Millam, J. M.; Schlegel, H. B. Ab Initio Classical Trajectories on the Born-Oppenheimer Surface: Updating Methods for Hessian-Based Integrators. *J. Chem. Phys.* **1999**, *111*, 8773−8777.
(49) Laaksonen, L. *Gopenmol, 3.0*; Center for Scientific Computing: Espoo, Finland, 2005, https://research.csc.fi/-/gopenmol.
(50) Jones, C. M.; Bernier, M.; Carson, E.; Colyer, K. E.; Metz, R.; Pawlow, A.; Wischow, E. D.; Webb, I.; Andriole, E. J.; Poutsma, J. C. Gas-Phase Acidities of the 20 Protein Amino Acids. *Int. J. Mass Spectrom.* **2007**, *267*, 54−62.
(51) Yao, Y.; Chen, D.; Zhang, S.; Li, Y.; Tu, P.; Liu, B.; Dong, M. Building the First Hydration Shell of Deprotonated Glycine by the Mcmm and Ab Initio Methods. *J. Phys. Chem. B* **2011**, *115*, 6213−6221.
(52) Michaux, C.; Wouters, J.; Perpète, E. A.; Jacquemin, D. Ab Initio Investigation of the Hydration of Deprotonated Amino Acids. *J. Am. Soc. Mass Spectrom.* **2009**, *20*, 632−638.
(53) Wincel, H. Hydration of Gas-Phase Protonated Alkylamines, Amino Acids and Dipeptides Produced by Electrospray. *Int. J. Mass Spectrom.* **2006**, *251*, 23−31.
(54) Eckersley, M.; Bowie, J. H.; Hayes, R. N. Collision-Induced Dissociations of Deprotonated α-Amino Acids. The Occurrence of Specific Proton Transfers Preceding Fragmentation. *Int. J. Mass Spectrom.* **1989**, *93*, 199−213.
(55) Waugh, R. J.; Bowie, J. H.; Gross, M. L. Collision-Induced Dissociation of Deprotonated Peptides. Dipeptides Containing Methionine or Cysteine. *Rapid Commun. Mass Spectrom.* **1993**, *7*, 623−625.
(56) Ervin, K. M.; Anusiewicz, I.; Skurski, P.; Simons, J.; Lineberger, W. C. The Only Stable State of O_2^- Is the $X^2\Pi_g$ Ground State and It (Still!) Has an Adiabatic Electron Detachment Energy of 0.45 eV. *J. Phys. Chem. A* **2003**, *107*, 8521−8529.
(57) Troe, J. Statistical Adiabatic Channel Model of Ion-Neutral Dipole Capture Rate Constants. *Chem. Phys. Lett.* **1985**, *122*, 425−430.
(58) O'Hair, R. A. J.; Reid, G. E. Neighboring Group Versus *Cis*-Elimination Mechansims for Side Chain Loss from Protonated Methionine, Methionine Sulfoxide and Their Peptides. *Eur. Mass Spectrom.* **1999**, *5*, 325.
(59) Rogalewicz, F.; Hoppilliard, Y.; Ohanessian, G. Fragmentation Mechanisms of α-Amino Acids Protonated under Electrospray Ionization: A Collisional Activation and ab Initio Theoretical Study. *Int. J. Mass Spectrom.* **2000**, *195/196*, 565−590.
(60) Rodgers, M. T.; Ervin, K. M.; Armentrout, P. B. Statistical Modeling of Collision-Induced Dissociation Thresholds. *J. Chem. Phys.* **1997**, *106*, 4499−4508.
(61) Zhu, L.; Hase, W. L. Comparison of Modes for Calculating the RRKM Unimolecular Constant K(E,J). *Chem. Phys. Lett.* **1990**, *175*, 117−124.
(62) Knickelbein, M. B.; Menezes, W. B. Optical Response of Small Niobium Clusters. *Phys. Rev. Lett.* **1992**, *69*, 1046−1049.
(63) Menezes, W. J. C.; Knickelbein, M. B. Photodissociation Spectroscopy of Nb_nAr_m Complexes. *J. Chem. Phys.* **1993**, *98*, 1856−1866.
(64) Gregoire, G.; Duncan, M. A. Infrared Spectroscopy to Probe Structure and Growth Dynamics in Fe^+-$(CO_2)_n$ Clusters. *J. Chem. Phys.* **2002**, *117*, 2120−2130.

DOI: 10.1021/acs.jpcb.5b03779
J. Phys. Chem. B 2015, 119, 8001−8012